ECCOMAS Thematic Conference on Computational Methods
in Structural Dynamics and Earthquake Engineering
M. Papadrakakis, D.C. Charmpis, N.D. Lagaros, Y. Tsompanakis (eds.)
Rethymno, Crete, Greece, 13–16 June 2007

A MIXED FINITE ELEMENT APPROACH FOR NONLINEAR DYNAMIC ANALYSIS OF COMPOSITE RECTANGULAR CONCRETE-FILLED STEEL TUBE (RCFT) FRAMES

Cenk Tort[1] **and Jerome F. Hajjar**[2]

[1] University of Minnesota
500 Pillsbury Drive SE Minneapolis, MN 55455 USA
e-mail: tort0008@umn.edu

[2] University of Illinois at Urbana-Champaign
205 North Mathews Ave Urbana, IL 61801 USA
e-mail: jfhajjar@uiuc.edu

Keywords: Composite, Mixed Finite Element, Structural Dynamics, Earthquake Engineering.

Abstract. *The worldwide progress to date in experimental and computational studies on composite frame structures having rectangular concrete-filled steel tube (RCFT) beam-columns and steel girders and braces has revealed their exceptional seismic resistance. In this paper, a computational study to develop reliability-based performance-based seismic design guidelines of RCFT members is presented. A three-dimensional geometrically and materially nonlinear mixed distributed-plasticity finite element formulation is developed for RCFT beam-columns as part of complete composite frame structures. The element stiffness matrices and internal forces are derived using a two-field mixed formulation, where deformation and stress-resultant fields along the element length are interpolated independently. Translational degrees-of-freedom for the steel tube and the concrete are defined separately to allow for differential slip displacement along the element length between the constituent materials, modeling cyclic interface and load transfer response ranging from perfect slip to complete bond. The material nonlinearity of the steel tube and the concrete core is accounted for through assigning comprehensive cyclic nonlinear stress-strain relations. Using an experimental database developed by the authors that documents detailed progression of damage in RCFT members and frames, a comprehensive verification study for the mixed finite element formulation is conducted on RCFT members under various loading conditions that highlights the complex interrelationship between the constitutive materials and the progression of damage with these composite members.*

1 INTRODUCTION

Based on the research experience initiated after the earthquakes of Northridge (1994) and Kobe (1995), it is well recognized that reliability-based performance-based design (PBD) methodologies enable engineers to produce structures with predictable seismic performance within prescribed levels of confidence [1]. Exhibiting promising features of large energy dissipation, strength, and stiffness, composite frames having RCFT columns and steel girders have become increasingly popular in mid-rise and high-rise buildings [2]. Developing PBD methods tailored with respect to the characteristics of such systems is critical in extending and spreading their use in earthquake prone regions.

In this paper, a finite element model of RCFT beam-columns is presented to be used for conducting nonlinear transient dynamic parametric studies of composite frames under earthquake loads to provide data for developing reliability-based performance-based design guidelines for RCFTs. A beam-column element is derived based on mixed-finite element principles following an Updated-Lagrangian distributed plasticity approach. The finite element formulation is able to capture a comprehensive range of behavioral features of RCFT beam-columns including flexural buckling, concrete confinement, local buckling of the steel tube, and cyclic constitutive characteristics of the steel and concrete. In addition, translational degrees-of-freedom for the steel tube and the concrete core are defined separately to allow for differential slip displacement along the element length between the constituent materials, modeling cyclic interface and load transfer response ranging from perfect slip to complete bond. The RCFT element formulation has been implemented in a general-purpose analysis framework and verified with respect to a wide range of available experimental results.

2 RCFT MIXED FINITE ELEMENT FORMULATION

Various finite element techniques have been formulated in the literature for second-order inelastic analysis of RCFT members. One dimensional (1D) line elements based on the Euler-Bernoulli beam-theory are often preferred to solid elements in order to reduce the computation time, which becomes important when analyzing large 3D frame structures subjected to dynamic loading. Available finite element models typically are either displacement-based [3, 4] or force-based [5] formulations relative to selecting the type unknown parameters approximated over the domain. This distinction of finite element models determines the accuracy and complexity of the methods to obtain element stiffness and internal forces. RCFT members exhibit nonlinear cyclic response attributed to both local and global geometric instability and several inelastic phenomena of the concrete core (e.g., concrete cracking, concrete crushing) and the steel tube (e.g., cyclic hardening, Bauschinger effect). Therefore, a rational simulation of the load-deformation response of RCFT members requires incorporating refined constitutive relations coupled with accounting for local and flexural buckling of the member.

In the current study, a mixed distributed plasticity beam-column element is derived to simulate the static, quasi-static, and transient dynamic response of RCFT members. Following the two field form of the Hellinger-Reissner variational principle, independent interpolation functions are introduced for both displacements and internal element forces [6]. This approach allows accurate representation of nonlinear curvature fields since it is possible to obtain realistic distributions of element internal forces [7]. Therefore, accuracy can be achieved with fewer finite elements along the element length compared to equivalent displacement-based formulations. Since internal element forces are interpolated along the element length, equilibrium is strictly satisfied. Force-based formulations exhibit similar characteristics as the mixed finite element formulations with respect to the estimation of

nonlinear curvature fields. However, the mixed finite element formulation alleviates the complexity of force-based formulations with respect to incorporating geometric nonlinearity and the slip response of RCFT members.

2.1 Kinematic Relations

In this RCFT formulation, the equations to derive the element stiffness matrix and internal forces are established within a corotational (natural) reference frame, where rigid body modes are excluded in the derivations. Shear deformations are neglected and a linear elastic torsional response is assumed along the element length. The cross-sectional deformations ($\boldsymbol{d}$ derived from cross-sectional forces, and $\hat{\boldsymbol{d}}$ derived from nodal displacements) along the element length are defined to include axial strains (ε) and curvatures (κ_y, κ_z) introduced for the steel tube and the concrete core separately. The deformation vectors $\boldsymbol{d}$ and $\hat{\boldsymbol{d}}$ are presented in Equations 1, where right superscripts "*s*" and "*c*" identify the quantities defined for the steel tube and the concrete core, respectively. Variables stated in bold represent either vector or matrix quantities. Due to the rotational compatibility (discussed in Section 2.2), the steel tube and the concrete core are assumed to attain the same curvature values.

$$\boldsymbol{d} = \left[\varepsilon^c \;\; \kappa_z^c \;\; \kappa_y^c \;\; \varepsilon^s \;\; \kappa_z^s \;\; \kappa_y^s\right]^T, \;\; \hat{\boldsymbol{d}} = \left[\hat{\varepsilon}^c \;\; \hat{\kappa}_z^c \;\; \hat{\kappa}_y^c \;\; \hat{\varepsilon}^s \;\; \hat{\kappa}_z^s \;\; \hat{\kappa}_y^s\right]^T \tag{1}$$

The axial strain is defined through the Green-Lagrange strain measure, which is expressed in terms of axial (u) and transverse deformation fields (v, w) as given in Equation 2. The curvatures are obtained by evaluating the second derivatives of the transverse deformation fields. In Equation 2, the operators "$,x$" and "$,xx$" denote differentiations to the first and second degree, respectively.

$$\varepsilon = u_{,x} + 0.5 \times \left(u_{,x}\right)^2 + 0.5 \times \left(v_{,x}\right)^2 + 0.5 \times \left(w_{,x}\right)^2, \;\; \kappa_z = v_{,xx}, \;\; \kappa_y = w_{,xx} \tag{2}$$

Similarly, the cross section forces ($\boldsymbol{D}$) are assumed to have axial force (P) and moment (M_y, M_z) components defined for the steel tube and the concrete core independently (Equation 3).

$$\boldsymbol{D} = \left[P^c \;\; M_z^c \;\; M_y^c \;\; P^s \;\; M_z^s \;\; M_y^s\right]^T \tag{3}$$

The force transfer between the steel tube and the concrete core is provided through a layer of nonlinear springs located at the interface. The deformation of the slip layer ($\hat{d}_{sc}$) is expressed in terms of axial deformation fields of the steel tube (u^s) and the concrete core (u^c) as stated in Equation 4. The stress generated at the interface (D_{sc}) is obtained through a cyclic constitutive relation assigned to the slip layer [4].

$$\hat{d}_{sc} = u^s - u^c \tag{4}$$

2.2 Finite Element Discretization

Adopting the prior work by [4], the proposed element has 18 global degree-of-freedoms (DOFs) with separate translational DOFs for the steel tube and the concrete core. At a single node with 9 DOFs, the first 3 DOFs correspond to steel translations. Since the concrete core is placed inside the steel tube, the rotations of the two media are assumed to be the same. Therefore, the second set of 3 DOFs represents both the steel tube and the concrete core rotations. The final 3 DOFs are defined for the concrete core translations. For an arbitrarily

oriented element in 3D space, differential movement can only occur in the axial direction due to lateral restraint provided by the steel tube. Therefore, shear translations of the steel tube and the concrete core are enforced to be equal to each other by the penalty function method [4]. This process is applied at the global level so that it does not exhibit any difference with respect to the type of finite element formulation.

In the natural coordinates, the nodal displacement vector ($\boldsymbol{q}$) is assumed to have a total of 13 DOFs including deformation of the slip layer (e^{sc}), axial deformations between the *i*-end and *j*-end of the element (e^s, e^c), rotations with respect to the *i*-end and *j*-end of the element ($\theta^c_{yi}, \theta^c_{yj}, \theta^c_{zi}, \theta^c_{zj}, \theta^s_{yi}, \theta^s_{yj}, \theta^s_{zi}, \theta^s_{zj}$), and axial deformations between the *i*-end and mid-joint of the element (e^c_m, e^s_m). The mid-joint, for which two axial deformations are assigned, is introduced to estimate the distribution of axial deformations accurately via higher order interpolation functions. The rotational DOFs in the natural coordinates are defined independently for the steel tube and the concrete core despite the fact that they are enforced to be the same. This type of decomposition of rotational natural DOFs allows the calculation of the concrete core and the steel tube shear forces during transformations into the global coordinates, where independent shear DOFs exist for the two media. The axial deformation fields along the element length are approximated in terms of natural nodal deformations through quadratic interpolation functions. The transverse deformation fields are interpolated along the element length using cubic Hermitian interpolation functions.

The energy equivalent nodal forces ($\boldsymbol{Q}$) corresponding to the natural nodal displacements include axial forces (P^c_i, P^c_j, P^s_i, P^s_i) and bending moments ($M^c_{yi}, M^c_{yj}, M^s_{yi}, M^s_{yj}, M^c_{zi}, M^c_{zj}, M^s_{zi}, M^s_{zj}$) defined at *i*-end and *j*-end of the element for the steel tube and the concrete core independently. The distributions of nodal forces along the element length are approximated using linear interpolation functions. However, the additional moments due to the $P\text{-}\delta$ effects are incorporated into the bending moment distributions [7].

Once the interpolation function approximations of the deformation fields are substituted into the kinematic relations in Equations 1 and 4, the cross-sectional strain measures can be represented in terms of the natural nodal displacement vector as given below:

$$\hat{\boldsymbol{d}} = \boldsymbol{N}_{\hat{d}} \times \boldsymbol{q}, \; \hat{d}_{sc} = \boldsymbol{N}_{\hat{d}_{sc}} \times \boldsymbol{q} \tag{5}$$

Similarly, introducing the interpolation functions defined for the axial forces and bending moments, Equation 6 is derived to express the cross-sectional forces in terms of nodal forces in the natural coordinates.

$$\boldsymbol{D} = \boldsymbol{N}_{D1} \times \boldsymbol{Q} \tag{6}$$

In Equations 5 and 6, the terms $\boldsymbol{N}_{\hat{d}}$, $\boldsymbol{N}_{\hat{d}_{sc}}$, and $\boldsymbol{N}_{D1}$ are the matrix quantities resulting from the process of introducing deformation and force distributions into the cross-section strain vector, slip-layer deformation, and cross-section force vector, respectively.

2.3 Element Equilibrium

The current formulation starts by expressing the virtual work equation of equilibrium as given in Equation 7, where the work done by the external loads is balanced by the internal stresses. Modeling the differential movement between the concrete core and the steel tube, the volumes of the two media are separated and an additional term is introduced to account for the energy due to slip. In the element equilibrium, the Updated-Lagrangian description of

motion is adopted such that all the kinematic and static variables of the current configuration (C2) are defined with respect to the most converged configuration (C1). The nomenclature by [8] is employed while developing the governing equations. Both left subscripts and superscripts identify the attained state of the solid body as either C1 or C2. A left superscript denotes the configuration in which the quantity takes place while a left subscript shows the configuration that the quantity is referred to. A variable defined with a subscript without any superscript is considered as an increment between the C1 and C2 configurations.

$$\int_0^{{}^1L} \delta_1\hat{\boldsymbol{d}}^T \times {}_1^2\boldsymbol{D} \times d^1x + \int_0^{{}^1L} \delta_1\hat{d}_{sc}^T \times {}_1^2D_{sc} \times d^1I + \int_{{}^1V^c} {}^1\rho^c \times {}_1^2\ddot{\boldsymbol{u}}^c \times \delta_1\boldsymbol{u}^c \times d^1V^c + \int_{{}^1V^s} {}^1\rho^s \times {}_1^2\ddot{\boldsymbol{u}}^s \times \delta_1\boldsymbol{u}^s \times d^1V^s + \int_{{}^1V^c} {}^1\mu^c \times {}_1^2\dot{\boldsymbol{u}}^c \times \delta_1\boldsymbol{u}^c \times d^1V^c + \int_{{}^1V^s} {}^1\mu^s \times {}_1^2\dot{\boldsymbol{u}}^s \times \delta_1\boldsymbol{u}^s \times d^1V^s - \delta_1\boldsymbol{q}^T \times {}_1^2\boldsymbol{Q}_{ext} = 0 \tag{7}$$

where I is the interface area, V is the element volume, ρ is the unit weight, μ is the viscosity parameter, $\dot{\boldsymbol{u}}$ is the velocity field, $\ddot{\boldsymbol{u}}$ is the acceleration field, $\boldsymbol{q}$ is the nodal displacement vector in natural coordinates, and $\boldsymbol{Q}_{ext}$ is the external load vector in natural coordinates

2.4 Compatibility

The compatibility equation of RCFT members can be stated in terms of cross-sectional strains as given Equation 8. Since both nodal displacements and internal forces are treated as primary variables, it is possible to obtain two sets of cross-sectional strains along the element length, $\boldsymbol{d}$ and $\hat{\boldsymbol{d}}$. Enforcement of the compatibility equation ensures having the same strain values from both nodal displacements and internal forces once a converged state is attained.

$$\int_0^{{}^1L} \delta_1^2\boldsymbol{D}^T \times ({}_1\hat{\boldsymbol{d}} - {}_1\boldsymbol{d}) \times d^1x = 0 \tag{8}$$

2.5 Hellinger-Reissner Variational Principle

The Hellinger-Reissner variational principle for the RCFT beam-column element can be derived by combining the element equilibrium and compatibility equations of Equations 7 and 8. Equations 5 and 6 are then substituted into the resulting expression and the final format of the Hellinger-Reissner variational principle becomes as given in Equation 9, where there exist two separate expressions. The terms of g and V correspond to the equilibrium and compatibility parts, respectively.

$$g = \begin{bmatrix} \int_0^{{}^1L} {}^1\boldsymbol{N}_{\delta\hat{d}}^T \times {}_1^2\boldsymbol{D} \times d^1x + \int_{{}^1I} {}^1\boldsymbol{N}_{\delta\hat{d}_{sc}}^T \times {}_1^2D_{sc} \times d^1I - {}_1^2\boldsymbol{Q}_{ext} + \int_0^{{}^1L} {}_1^2\boldsymbol{N}_{D2}^T \times ({}_1\hat{\boldsymbol{d}} - {}_1\boldsymbol{d}) \times d^1x + \\ \left(\int_{{}^1V^c} {}^1\rho^c \times {}^1\boldsymbol{N}_u^{cT} \times {}^1\boldsymbol{N}_u^c \times d^1V^c + \int_{{}^1V^s} {}^1\rho^s \times {}^1\boldsymbol{N}_u^{sT} \times {}^1\boldsymbol{N}_u^s \times d^1V^s \right) \times {}_1^2\ddot{\boldsymbol{q}} + \\ \left(\int_{{}^1V^c} {}^1\mu^c \times {}^1\boldsymbol{N}_u^{cT} \times {}^1\boldsymbol{N}_u^c \times d^1V^c + \int_{{}^1V^s} {}^1\mu^s \times {}^1\boldsymbol{N}_u^{sT} \times {}^1\boldsymbol{N}_u^s \times d^1V^s \right) \times {}_1^2\dot{\boldsymbol{q}} \end{bmatrix} = 0 \quad , \; V = \int_0^{{}^1L} {}_1^2\boldsymbol{N}_{D1}^T \times ({}_1\hat{\boldsymbol{d}} - {}_1\boldsymbol{d}) \times d^1x = 0 \tag{9}$$

In Equation 9, $\boldsymbol{N}_{\delta\hat{d}}$ and $\boldsymbol{N}_{\delta\hat{d}_{sc}}$ are obtained as the first variations of $\boldsymbol{N}_{\hat{d}}$ and $\boldsymbol{N}_{\hat{d}_{sc}}$, respectively. $\boldsymbol{N}_{D2}$ can be derived by manipulating the expressions from the first variation of $\boldsymbol{N}_{D1}$ ($\delta\boldsymbol{D} = \boldsymbol{N}_{D2} \times \delta\boldsymbol{q} + \boldsymbol{N}_{D1} \times \delta\boldsymbol{Q}$). $\boldsymbol{N}_u^c$ and $\boldsymbol{N}_u^s$ are derived once the velocity and acceleration fields of the concrete core and the steel tube are expressed in terms of their nodal values ($\dot{\boldsymbol{q}}$ is

the nodal velocity in natural coordinates, $\ddot{\boldsymbol{q}}$ is the nodal displacement in natural coordinates) with the use of deformation interpolation functions described in Section 2.2.

In the current formulation, the cross-section forces can be obtained based on two different methods. The nodal forces are interpolated along the element length as defined in Equation 6 to obtain $\boldsymbol{D}$. In addition, cross-section forces ($\boldsymbol{D}_\Sigma$) can also be calculated by performing numerical integration of the stresses generated at the material fibers. The balance between these two sets of forces must be satisfied along with the element equilibrium and compatibility equations. The mathematical expression of the equilibrium equation at the cross-section level ($\boldsymbol{U}$) is stated below.

$$\boldsymbol{U} = {}^{2}_{1}\boldsymbol{D}_\Sigma - {}^{2}_{1}\boldsymbol{D} = 0 \tag{10}$$

The nonlinear nature of Equations 9 and 10 requires the solution of element displacements and forces through an incremental-iterative algorithm. Performing linearization of the aforementioned equations, the stiffness matrices and internal force expressions are derived. The linearization process is conducted by expanding the equations about their current state with respect to the their state variables $\boldsymbol{D}$, $\boldsymbol{d}$, $\boldsymbol{q}$, $\dot{\boldsymbol{q}}$, $\ddot{\boldsymbol{q}}$, $\boldsymbol{Q}$, and $\boldsymbol{Q}_{ext}$. The internal forces are derived using the linearized forms of Equations 9 and 10 such that while executing the incremental-iterative algorithm, the resulting unbalances are transferred to the next iteration until convergence is achieved at the global level.

2.6 Element Stiffness

The element stiffness matrix is calculated at the beginning of every iteration (j) in a time step (i). Assembling the global stiffness matrix, the incremental nodal displacements ($\Delta\boldsymbol{q}$) corresponding to the given time step can be solved. As given in Equation 11, the terms of the element stiffness matrix ($\boldsymbol{K}$) are derived from linearization of the element equilibrium expression (g) in Equation 9.

$${}^{2}_{1}\boldsymbol{K}^{j}_{i} = \begin{bmatrix} \left({}^{2}_{1}\boldsymbol{K}^{j}_{g} + {}^{2}_{1}\boldsymbol{K}^{j}_{sc} + \boldsymbol{G}^{j}_{2} + \left(\boldsymbol{G}^{T}_{2}\right)^{j} - {}^{2}_{1}\boldsymbol{H}^{j}_{22} \right) + \\ \left(\left(\boldsymbol{G}^{T}_{1}\right)^{j} + \left(\boldsymbol{M}^{T}_{d}\right)^{j} - \left({}^{2}_{1}\boldsymbol{H}^{T}_{12} \right)^{j} \right) \times {}^{1}\left({}^{2}_{1}\boldsymbol{H}^{-1}_{11} \right)^{j} \times \left(\boldsymbol{G}^{j}_{1} + \boldsymbol{M}^{j}_{d} - {}^{2}_{1}\boldsymbol{H}^{j}_{12} \right) \end{bmatrix} \tag{11}$$

where ${}^{2}_{1}\boldsymbol{K}_{g}$ is the geometric stiffness matrix [4], ${}^{2}_{1}\boldsymbol{K}_{sc} = \left[\int_{0}^{{}^{1}L} {}^{1}\boldsymbol{N}^{T}_{\delta\hat{d}_{sc}} \times {}^{2}_{1}\bar{k}^{j}_{sc} \times {}^{1}\boldsymbol{N}_{\delta\hat{d}_{sc}} \times d^{1}x \right]$ ($\bar{k}_{sc}$ is the stiffness of the slip layer (force/length^3)), ${}^{2}_{1}\boldsymbol{G}_{1} = \int_{0}^{{}^{1}L} {}^{2}_{1}\boldsymbol{N}^{T}_{D1} \times {}^{1}\boldsymbol{N}_{\delta\hat{d}} \times d^{1}x$, ${}^{2}_{1}\boldsymbol{G}_{2} = \int_{0}^{{}^{1}L} {}^{1}\boldsymbol{N}^{T}_{\delta\hat{d}} \times {}^{2}_{1}\boldsymbol{N}_{D2} \times d^{1}x$, ${}^{2}_{1}\boldsymbol{H}_{11} = \int_{0}^{{}^{1}L} {}^{2}_{1}\boldsymbol{N}^{T}_{D1} \times {}^{2}_{1}\boldsymbol{k}^{-1} \times {}^{2}_{1}\boldsymbol{N}_{D1} \times d^{1}x$ ($\boldsymbol{k}$ is the cross-section stiffness [4]), ${}^{2}_{1}\boldsymbol{H}_{12} = \int_{0}^{{}^{1}L} {}^{2}_{1}\boldsymbol{N}^{T}_{D1} \times {}^{2}_{1}\boldsymbol{k}^{-1} \times {}^{2}_{1}\boldsymbol{N}_{D2} \times d^{1}x$, $\boldsymbol{M}_d$ is the matrix resulting from linearization of the compatibility expression (V)

2.7 Element Internal Force

In an incremental-iterative nonlinear analysis, the determination of internal element forces is required to check the convergence of the current solution. In addition, recovery of the internal element forces is needed to update the terms of the geometric stiffness matrix [8]. A

summary of the steps to obtain the internal element load vector is portrayed in Figure 1 assuming that the analysis is proceeding from j^{th} iteration to j+1 iteration of a single time step. In the current formulation, the element internal force determination initiates as the incremental nodal displacements ($\Delta \boldsymbol{q}$) are obtained. The cross-section strain vectors ($\hat{\boldsymbol{d}}$) and slip layer deformations ($\hat{\boldsymbol{d}}_{sc}$) are updated by substituting $\Delta \boldsymbol{q}$ into the kinematic relations described in Section 2.1. The incremental nodal forces ($\Delta \boldsymbol{Q}$) are determined by multiplying the inverse of the element flexibility ($\boldsymbol{H}_{11}^{-1}$) with the compatibility expression of Equation 9. Updating the nodal force vector ($\boldsymbol{Q}$), the cross-section forces ($\boldsymbol{D}$) are determined by means of force interpolation functions. The cross-section equilibrium described in Equation 10 is evaluated and the resulting unbalances are multiplied by the inverse of the cross-section stiffness ($\boldsymbol{k}^{-1}$) to obtain the cross-section strain vectors ($\boldsymbol{d}$). Despite the fact that slip deformation violates the assumption of plane-sections remaining plane, the strain profile of the cross section is still taken as linear while calculating the strains of the steel and concrete fibers of the RCFT cross-section. The constitutive relations defined for the steel and concrete fibers are utilized to obtain the cross-section force vector ($\boldsymbol{D}_{\Sigma}$) and cross-section stiffness matrix ($\boldsymbol{k}$) through numerical integration over the material fibers. The constitutive relation assigned to the slip layer is used to update the stiffness of the interface ($\bar{k}_{sc}$). The information acquired up to this point is sufficient to calculate the terms described in the 6th step of Figure 1. These terms are then used to quantify the expression of the element internal forces in the 7th step of Figure 1.

3 CONSTITUTIVE RELATIONS

The material nonlinearity of the RCFT member is simulated employing a fiber-based distributed plasticity approach. The element cross-sections located at the interpolation points are divided into individual steel and concrete fibers. Each material fiber is associated with a cyclic constitutive relation that is traced throughout the analysis.

The confinement in RCFT members is not considered to cause an enhancement in the compressive strength of concrete. However, the ductility achieved by the concrete core is significantly improved. In this research, the uniaxial cyclic concrete model by [9] is adapted for RCFT members. Envelope curves define the boundaries of the stress-strain response in tension and in compression. The stress-strain response ranging from the compression to tension envelope is represented through connecting curves. Transition curves simulate the shift between the connecting curves going in opposite directions. The negative envelope curve of RCFT members were derived by [10] based on the axially-loaded column tests in the literature. An ascending stress-strain response similar to that of plain concrete is assumed until the attainment of the peak compressive strength. The ascending response is followed by a linear softening region where the degradation slope is derived as a function of the compressive strength of the concrete core and slenderness of the steel tube. At high strain levels, the compressive envelope curve is assumed to undergo a constant stress region. The cyclic rules represented by the connecting and transition curves are kept largely as provided by [9]. However, the existing cyclic rules were augmented through introducing several new rules to capture the complex strain histories that RCFT members experience during quasi-static and dynamic loading conditions. For example, new unloading and reloading curves are introduced as presented in Figure 2, which define the cyclic rule following an unloading type response at the strain levels beyond the latest unloading strain prior to reaching to the target strain on the envelope curves.

1. Update nodal displacements ${}_1\boldsymbol{q}^{j+1}$ and cross-section strain ${}_1\hat{\boldsymbol{d}}^{j+1}$ (Equation 5)
2. Evaluate incremental element forces, $\Delta\boldsymbol{Q}^{j+1} = \left({}^2_1\boldsymbol{H}_{11}^{-1}\right)^j \times \boldsymbol{V}^j$, where:

$$\boldsymbol{V}^j = \int_0^{{}^1L} {}^2_1\left(\boldsymbol{N}_{D1}^T\right)^j \times \left({}_1\hat{\boldsymbol{d}}^{j+1} - {}_1\boldsymbol{d}^j - {}^2_1\left(\boldsymbol{k}^{-1}\right)^j \times \left({}^2_1\boldsymbol{D}^j - {}^2_1\boldsymbol{D}_\Sigma^j\right)\right) \times d^1x$$

3. Update element nodal forces (${}^2_1\boldsymbol{Q}^{j+1}$) and cross-section forces (${}^2_1\boldsymbol{D}^{j+1}$) (Equation 6)
4. Evaluate the cross-section strain vectors from nodal forces

$${}_1(\boldsymbol{d})_k^{j+1} = {}^2_1\left(\boldsymbol{k}^{-1}\right)_k^j \times \left({}^2_1(\boldsymbol{D})_k^{j+1} - {}^2_1\left(\boldsymbol{D}_\Sigma\right)_k^j\right) \text{ for } (k = 1; k \le \textit{Number of Sections})$$

5. Evaluate ${}^2_1\boldsymbol{k}_k^{j+1}$, ${}^2_1\left(\bar{k}_{sc}\right)_k^{j+1}$, ${}^2_1\left(\boldsymbol{D}_\Sigma\right)_k^{j+1}$ for ($k = 1$; $k \le$ *Number of Sections*)
6. Evaluate ${}^2_1\boldsymbol{G}_1^{j+1}$, ${}^2_1\boldsymbol{K}_{sc}^{j+1}$, $\int_{{}^1I} {}^1\boldsymbol{N}_{\delta\hat{d}_{sc}}^T \times {}^1\boldsymbol{D}_{sc} \times d^1I$, $\int_0^{{}^1L} {}^2_1\left(\boldsymbol{N}_{D2}^T\right)^{j+1} \times ({}_1\hat{\boldsymbol{d}}^{j+1} - {}_1\boldsymbol{d}^{j+1}) \times d^1x$, ${}^1\boldsymbol{M}_d$, ${}^2_1\left(\boldsymbol{H}_{11}\right)^{j+1}$, ${}^2_1\left(\boldsymbol{H}_{12}\right)^{j+1}$, $\boldsymbol{V}^{j+1}$ (see Equations 9, 10, 11)
7. Evaluate the element internal forces

$${}^2_1\boldsymbol{Q}_{int}^{j+1} = {}^2_1\left(\boldsymbol{G}_1^T\right)^{j+1} \times {}^2_1\boldsymbol{Q}^{j+1} + {}^2_1\boldsymbol{K}_{sc}^{j+1} \times {}_1\boldsymbol{q}^{j+1} + \int_{{}^1I} {}^1\left(\boldsymbol{N}_{\delta\hat{d}_{sc}}^T\right) \times {}^1\boldsymbol{D}_{sc} \times d^1I +$$

$$\int_0^{{}^1L} {}^2_1\left(\boldsymbol{N}_{D2}^T\right)^{j+1} \times ({}_1\hat{\boldsymbol{d}}^{j+1} - {}_1\boldsymbol{d}^{j+1}) \times d^1x + \left({}^2_1\left(\boldsymbol{G}_1^T\right)^{j+1} + \boldsymbol{M}_d^T - {}^2_1\left(\boldsymbol{H}_{12}^T\right)^{j+1}\right) \times {}^2_1\left(\boldsymbol{H}_{11}^{-1}\right)^{j+1} \times \boldsymbol{V}^{j+1}$$

Figure 1: Determination of internal element forces.

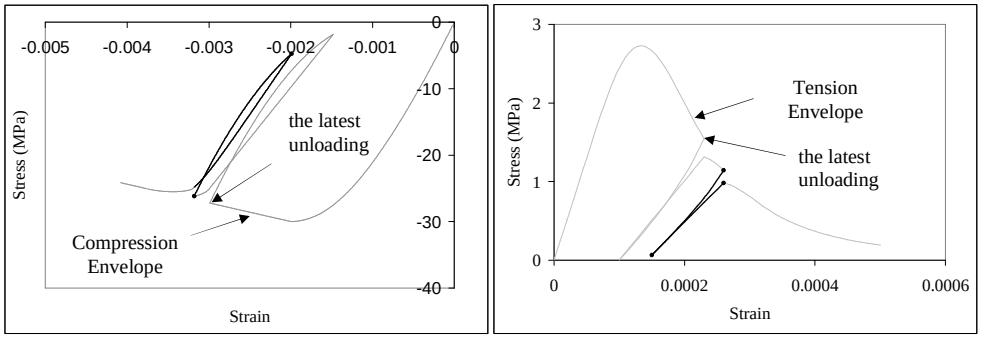

Figure 2: Unloading response between the latest unloading points and the envelope curves.

The uniaxial bounding surface model by [11] is adopted to simulate the cyclic stress-strain response of the steel tube of RCFT members. The phenomena of gradual stiffness reduction, reduction in the elastic zone, and the Bauschinger effect are accounted for in the model. The scope of the current research study is limited to RCFT members having cold-formed steel tubes. Therefore, the model by [11] was modified to include the effect of residual stresses by introducing a different initial plastic strain (ε_{po}) for the flat and corner regions of the steel tube, as shown in Figure 3. Local buckling of the steel tube is accounted for assuming a linear strength degradation once the plastic strain (ε_p) exceeds a limiting value of ε_{plb} as can be seen in Figure 3.

4 VERIFICATION STUDIES

The mixed finite element formulation developed for RCFT beam-columns is implemented in [12] along with the steel and concrete cyclic constitutive relations. In addition, a steel

beam-column element is also developed and implemented using the mixed finite element principles to serve as girders in composite frames.

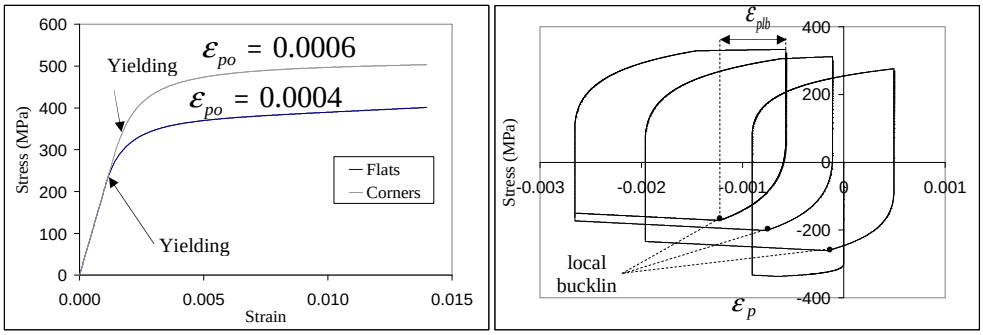

Figure 3: Residual stress and local buckling behavior of the steel tube.

A wide range of experiments on RCFT members and frames were used to verify the formulation; five are reported here. The first verification study is conducted on a non-proportionally loaded RCFT beam-column tested by [13]. The specimen is subjected to a constant axial load and uniform bending moment. Pinned and roller support conditions are introduced at the ends of the specimens. The analysis is performed using the Newton-Raphson solution scheme with constant displacement arc-length method near the limit point of the analysis [8]. In Figure 4, the comparison of experimental and computational results is presented. The measured material and geometric properties of the specimens are also given including yield strength of the steel tube (f_y), compressive strength of concrete (f'_c), depth (D) over thickness (t) ratio, length (L) over depth ratio (D), and axial load ratio (P / P_o). It is found that using 2 elements per member with 3 integration points produced satisfactory results. The second verification study is performed on a proportionally-loaded simply-supported RCFT column, where two steel girders are connected at the mid-height through shear tabs [14]. The loading condition involves an axial loading at the top of the RCFT column that is increased in proportion to the shear loading acting on both of the steel girders. The shear loading is transferred to the concrete core through the interface of the steel tube and the concrete core. In Figure 4, the comparison of the slip response along the element length is presented. The mesh size is determined based on the reported slip data. For an analysis conducted with 10 elements and 3 integration points, a good correlation is achieved between the experimental and computational results. Quasi-static cyclic simulations are then shown for two RCFT specimens from the literature [15-16]. The first specimen is a 3D subassembly with steel girders framing into an RCFT beam-column in two perpendicular directions simulating a 3D loading condition [16]. A pinned-RCFT column is subjected to a constant axial load at the top. A constant gravity load is applied on to the steel girder framing to the RCFT column in the out-of-plane direction. Antisymmetric cyclic shear loading is generated through the steel girders that are in plane with the RCFT column. The steel girders are modeled with 1 element and 3 integration points and the RCFT column is simulated through 2 elements and 3 integration points. The cyclic shear load vs. drift rotation response obtained from the analysis and the experiment exhibits a strong correlation as shown in Figure 5. A portal frame specimen having two RCFT columns and a steel girder in between is analyzed under constant axial load and cyclically applied shear loading, putting the columns into double curvature [16]. Both the RCFT columns and the steel girder are modeled using 3 elements and 3 integration points. As can be seen from Figure 5, the analysis estimated the

experimental shear vs. drift ratio response with good accuracy. The final verification example involves a nonlinear time-history analysis of an approximately half-scale multistory RCFT frame by [17] as portrayed in Figure 6. The structure was subjected to acceleration records using the pseudo-dynamic testing method. In the analysis model, 3 elements per member with 3 integration points and 4 elements per member with 3 integration points are used for the RCFT columns and steel girders, respectively. The Newmark-Beta (γ = 0.5, β = 0.25) time integration method is employed to solve for the response of the structure. The 1994 Northridge-Canoga Park acceleration record scaled to the design basis response spectra is applied to the structure. The mass of the structure is assumed to be lumped to the nodes of the leaning column at the story heights. The leaning column is connected to the structure through rigid links attached to the mid-point of the girders at the both bays of the structure. Stiffness and mass proportional damping are introduced with proportionality factors of 0.001194 and 0.154667, respectively, as recommended by [17]. The measured geometric and material properties of structural members are utilized in the analysis. The comparison of experimental and computational results is performed with respect to story shear vs. drift response of the structure. As can be seen from Figure 7, good correlation is achieved between the two sets of the data for 1st and 2nd story of the structure.

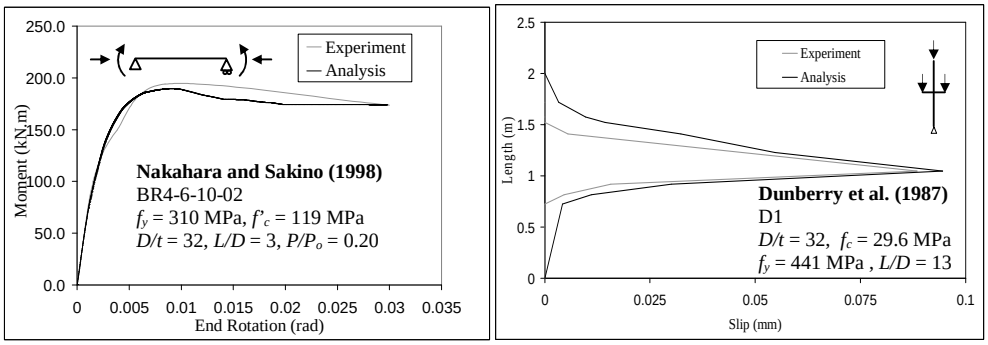

Figure 4: Non-proportionally loaded RCFT beam-columns.

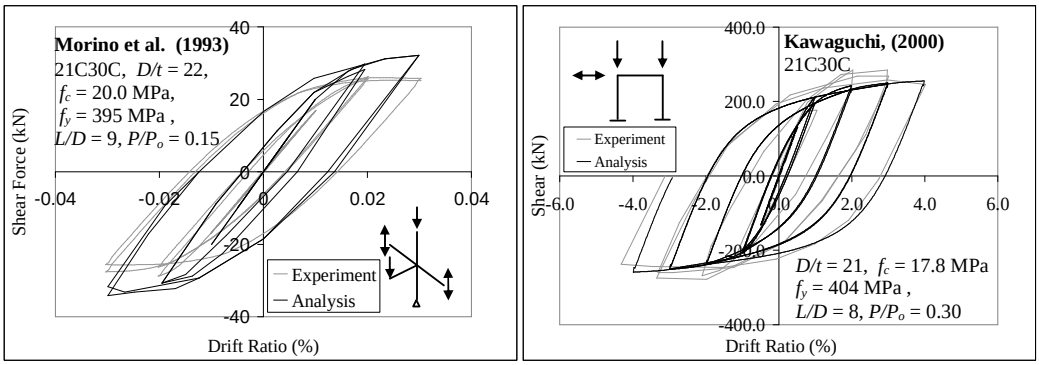

Figure 5: Non-proportionally loaded RCFT beam-columns.

5 CONCLUSIONS

A new mixed finite element formulation is introduced for fully nonlinear static and dynamic analysis of RCFT frames. The following remarks can be inferred from the analysis results using the proposed formulation:

- The mixed finite element formulation is capable of producing accurate and robust simulations of RCFT beam-columns experiencing inelastic curvatures. Utilizing 2

finite elements per member with 3 interpolation points often yielded satisfactory comparisons with the experiments both in the hardening and softening regions of the load deformation response.

- The constitutive relations adopted for the steel tube and the concrete core capture the limit states of concrete cracking, concrete crushing, and local buckling of the steel tube with acceptable accuracy. They are found to be robust even under complicated strain histories resulting from the irregularity of the ground motion records.
- This formulation is suitable for analyzing complete three-dimensional composite frame structures, including either braced or unbraced, subjected to static or transient dynamic loading. The formulation includes modeling of differential slip between the steel tube and concrete core in the RCFT, which is particularly important in the connection regions of braced frames.

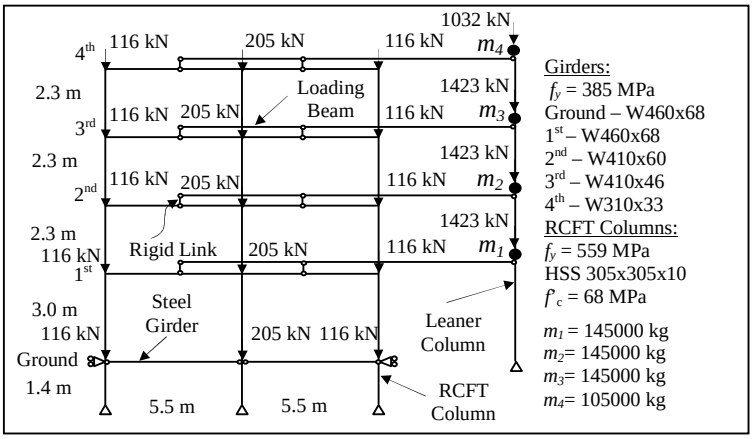

Figure 6: RCFT test structure by Herrera [17].

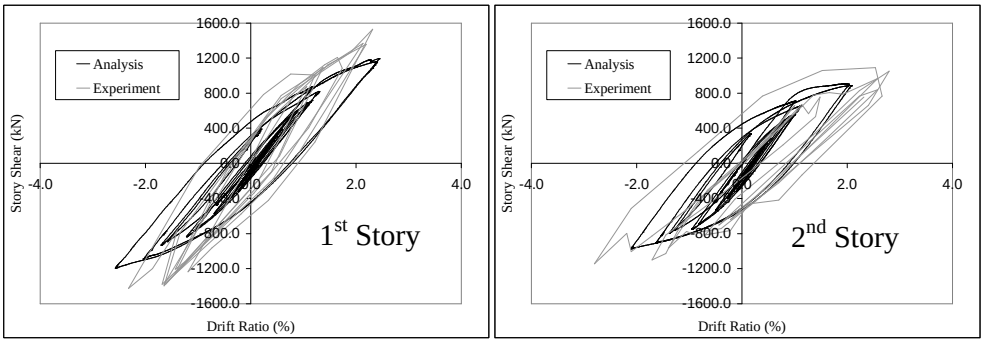

Figure 7: Story shear vs. story drift response.

REFERENCES

[1] S. Yun, R. O. Hamburger, C. A. Cornell, D. A. Foutch, Seismic performance evaluation for steel moment frames, *Journal of Structural Engineering*, **128**, 4, 534-545, 2002.

[2] J. F. Hajjar, Composite steel and concrete structural systems for seismic engineering. *Journal of Constructional Steel Research,* **58**, 5-8, 703-728, 2002.

[3] J. F. Hajjar, B. C. Gourley, A cyclic nonlinear model for concrete-filled tubes. I. Formulation. II. Verification, *Journal of Structural Engineering*, **123**, 6, 736-754, 1997.

[4] J. F. Hajjar, A. Molodan, P. H. Schiller, A distributed plasticity model for cyclic analysis of concrete-filled steel tube beam-columns and composite frames, *Engineering Structures*, **20**, 4-6, 398-412, 1998.

[5] A. H. Varma, J. M. Ricles, R. Sause, L. Lu, Seismic behavior and modeling of high-strength composite concrete-filled steel tube (CFT) beam-columns. *Journal of Constructional Steel Research*, **58**, 5-8, 725-758, 2002.

[6] O. C. Zienkiewicz, R.C. Taylor, J. Z. Zhu, *The finite element method, Vol. I, 6th Edition*. Elsevier, Oxford, U.K., 2005.

[7] B. N. Alemdar, D. W. White, Displacement, flexibility, and mixed beam-column finite element formulations for distributed plasticity analysis. *Journal of Structural Engineering*, **131**, 12, 1811-1819, 2005.

[8] Y. B. Yang, S. R. Kuo, *Theory and analysis of nonlinear framed structures*. Prentice Hall, Englewood Cliffs, New Jersey, 1994.

[9] G. A. Chang, J. B. Mander, Seismic energy based fatigue damage analysis of bridge columns: Part I – Evaluation of seismic capacity, Technical Report NCEER-94-0006, Department of Civil Engineering, State University of New York, Buffalo, New York, 1994.

[10] C. Tort, J. F. Hajjar, Damage assessment for performance-based design of rectangular concrete-filled steel tubes. *Composite Construction in Steel and Concrete V*, Virginia: United Engineering Foundation, American Society of Civil Engineers, Reston, Virginia, 2004.

[11] E. Mizuno, C. Shen, Y. Tanaka, T. Usami, A uniaxial stress-strain model for structural steels under cyclic loading, *Stability and Ductility of Steel Structures Steels under Cyclic Loading*, Boca Raton, Florida, 37-48, 1992.

[12] OpenSEES, Open System for Earthquake Engineering Simulation. Pacific Earthquake Engineering Research Center, University of California at Berkeley, Berkeley, California, 1999.

[13] H. Nakahara, K. Sakino, Axial compressive and uniform bending tests of high strength concrete filled square steel tubular columns, *The Fifth Pacific Structural Steel Conference*, Seoul, Korea, October 13-16, 1998, 943-948, 1998.

[14] E. Dunberry, D. LeBlanc, R. G. Redwood, Cross-section strength of concrete-filled HSS columns at simple beam connections, *Canadian Journal of Civil Engineering*, **14**, 408–417, 1987.

[15] S. Morino, J. Kawaguchi, C. Yasuzaki, S. Kanazawa, Behavior of concrete-filled steel tubular three-dimensional subassemblages, *Composite Construction in Steel and Concrete II*, New York, New York, 726-741, 1993.

[16] J. Kawaguchi, S. Morino, T. Sugimoto, J. Shirai, Experimental study on structural characteristics of portal frames consisting of square CFT columns," *Composite Construction in Steel and Concrete IV*, United Engineering Foundation, American Society of Civil Engineers, Reston, Virginia.

[17] L. A. Herrera, Seismic behavior of concrete-filled tube columns-wide flange beam frames, Ph.D. Dissertation, Dept. of Civil Engineering, Lehigh University, Bethlehem, Pennsylvania, 2005.